Ultrafast Graphene Oxide Humidity Sensors

Stefano Borini,* Richard White, Di Wei, Michael Astley, Samiul Haque, Elisabetta Spigone, Nadine Harris, Jani Kivioja, and Tapani Ryhänen

Nokia Research Center, 21 JJ Thomson Avenue, Madingley Road, Cambridge CB3 0JE, United Kingdom

ABSTRACT Sensors allow an electronic device to become a gateway between the digital and physical worlds, and sensor materials with unprecedented performance can create new applications and new avenues for user interaction. Graphene oxide can be exploited in humidity and temperature sensors with a number of convenient features such as flexibility, transparency and suitability for large-scale manufacturing. Here we show that the two-dimensional nature of graphene oxide and its superpermeability to water combine to enable humidity sensors with unprecedented response speed (~30 ms response and recovery times). This opens the door to various applications, such as touchless user interfaces, which we demonstrate with a 'whistling' recognition analysis.

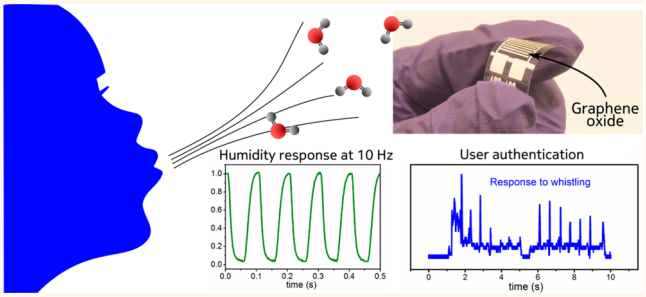

KEYWORDS: graphene · graphene oxide · 2D materials · sensors

Graphene is only the first of a new class of two-dimensional (2D) crystals with unique properties,[1] which are being investigated and deployed with increasing vigor in various fields such as electronics and optoelectronics.[2−4] Moreover, functionalized graphene materials provide a further set of 2D materials with exceptional promise for biological and chemical sensors.[5−8] Graphene oxide (GO) is a graphene derivative where oxygen-containing functional groups, such as epoxy, hydroxyl, and carboxyl groups, cover the surface,[9] turning the material into an electrical insulator. Although graphite oxide has been known since 1855,[10] a heightened interest in GO was triggered by the explosion in graphene research activity starting in 2004.[11,12] Ruoff and coauthors reported the exceptional mechanical properties of graphene oxide paper,[13] made by the assembly of individual GO sheets. Recently Nair and coauthors demonstrated a selective superpermeability of GO membranes to water molecules,[14] suggesting new applications such as water filtration. The interaction of GO with water molecules is particularly interesting because, in addition to the observed superpermeability, aqueous solutions of GO are also observed to be acidic.[15] Protons generated *via* the reaction of water molecules with the GO surface functional groups produce a decrease in the electrical impedance.[16] Therefore, the interaction of GO with water molecules can be deployed in humidity sensing devices.[17−21]

Here we show that the distinctive 2D structure of GO, combined with its superpermeability to water molecules, leads to sensing devices with an unprecedented speed. The GO-based sensors reported here exhibit a number of convenient features such as transparency, flexibility and suitability for large-scale manufacturing. The ultrafast response speed of these sensors allows us to observe the modulation of moisture in a user's breath, and we demonstrate this feature in a whistled tune recognition application. Moreover, the same concept may be explored in the case of different 2D materials, such as functionalized graphene and 2D transition metal dichalcogenides, in interaction with different vapors and gases for the realization of ultrathin nanoporous films for sensing applications.

RESULTS AND DISCUSSION

Analysis of GO Impedance Spectrum and Humidity Sensing Behavior. We studied the effect of water molecules on the electrical properties of GO films of variable thickness by

* Address correspondence to stefano.borini@nokia.com.

Received for review September 18, 2013 and accepted November 9, 2013.

Published online November 09, 2013
10.1021/nn404889b

© 2013 American Chemical Society

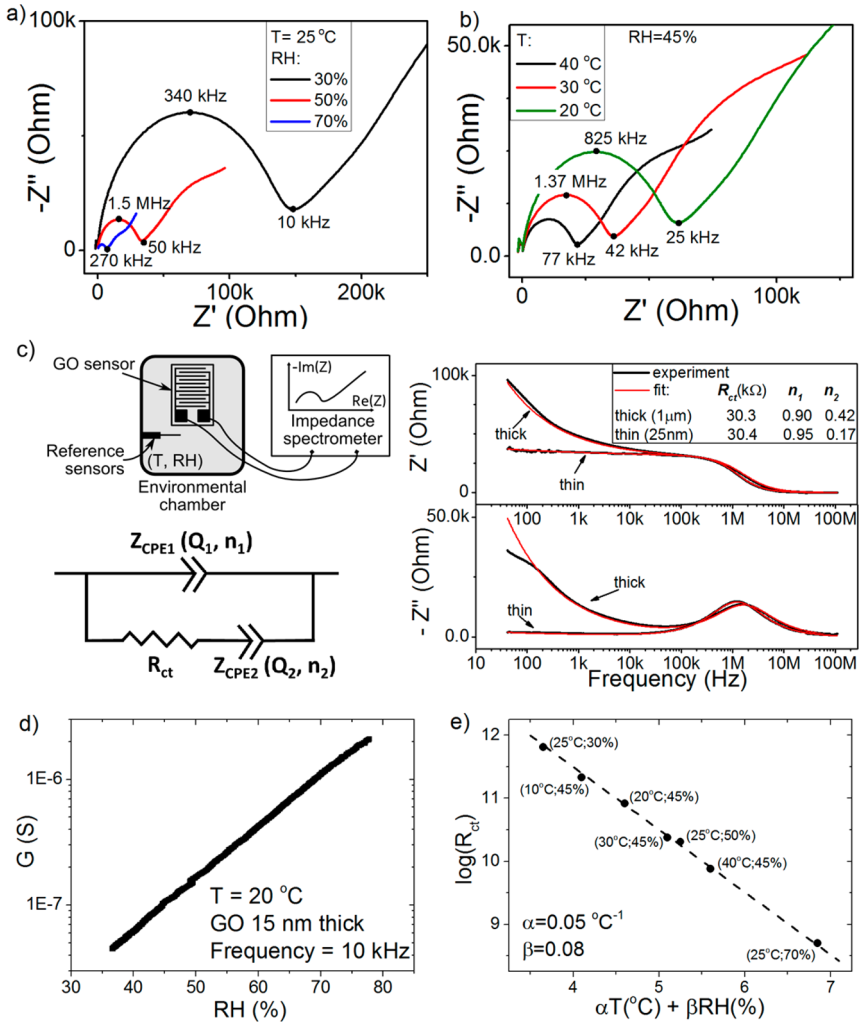

Figure 1. (a and b) Nyquist plots of the impedance (imaginary part Z'' *versus* real part Z' within the frequency range 40 Hz to 110 MHz) of a drop cast GO film at various RH and T conditions; (c) diagram of the experimental setup and fitting of the impedance spectrum, by using the displayed equivalent circuit, for two different GO film thickness values (RH = 50% for the thick film and 70% for the thin film, T = 25 °C); (d) conductance response of an ultrathin GO film to RH variation; (e) exponential behavior of the R_{ct} parameter *vs* both humidity and temperature according to eq 2, for a drop cast GO film.

extensive impedance measurements in an environmental chamber, where the temperature (T) and relative humidity (RH) were varied in a controlled way (T range 10−40 °C, RH range 30−80%). GO films were deposited by either drop casting or spray coating on top of silver screen-printed interdigitated electrodes on a polyethylene naphthalate (PEN) substrate. Three types of GO films with different thickness values were studied: ultrathin spray-coated film (0.2 mL sprayed volume, ∼15 nm thick), thin spray-coated (1 mL sprayed, ∼25 nm thick) and thick drop cast (thickness ≥1 μm). The thickness values were estimated by combination of Atomic Force Microscopy (AFM), optical absorption and Scanning Electron Microscopy (SEM). Details about film thickness evaluation are given in the Supporting Information. The reproducibility of all the observations reported in this study was checked by testing several samples for each type of film.

As shown in Figure 1a,b, the GO impedance spectrum is very sensitive to both RH and T. To a first approximation, the impedance spectrum of the GO samples can be modeled by the equivalent circuit shown in Figure 1c, including a charge transfer resistance R_{ct} and two constant phase elements CPE1 and CPE2. The impedance of a constant phase element Z_{CPE} is generally defined as

$$Z_{CPE} = Q^{-1}(i\omega)^{-n} \quad 0 \le n \le 1 \qquad (1)$$

where Q is a real parameter, i the imaginary unit, ω the frequency, and n a real parameter whose value can vary from 0 (pure resistor) to 1 (pure capacitor).

In the case of our GO samples, the value of n, obtained by best fit of the impedance spectra, was always very close to 1 for the constant phase element CPE1, varying from 0.90 to 0.97 (*i.e.*, becoming an almost pure capacitor) with decreasing film thickness, while in the case of CPE2, the value of n varied from 0.4 (drop cast GO films) to 0.2 (1 mL spray-coated) to almost 0 for ultrathin films (0.2 mL spray-coated). Such evolution of the impedance spectrum with the GO film

thickness is highlighted in Figure 1c, where we show that, although in some cases the same R_{ct} value can be obtained for GO films with different thickness, the spectra are yet markedly distinct, due to the different relevance of the diffusion phenomena in thick and thin samples. Thus, the same general equivalent circuit could be used to describe various GO films with different thicknesses. The behavior of both constant phase elements points out that, with reducing the GO thickness down to ultrathin GO films, the equivalent circuit tends to become a simple *RC* circuit. The standard Randles circuit (proposed, *e.g.*, in ref 16) was found unable to reproduce the whole range of the analyzed impedance spectra; that is, it could not represent the spectrum of GO films within the whole range of thicknesses. More complex equivalent circuits, including more elements, might be able to fit the experimental spectra with better accuracy in the low frequency region; such a study is ongoing and beyond the aim of this paper.

Upon changing RH and/or *T*, only two parameters in the equivalent circuit of Figure 1c are affected for a given sample: the charge transfer resistance R_{ct} and the parameter *Q* of the constant phase element CPE2, which can both be used as sensing parameters. In particular, we have observed that the dependence of R_{ct} on RH and *T* can be approximated by an exponential relationship (see Figure 1e), which can be expressed in the following form:

$$\log(R_{ct0}/R_{ct}) = \alpha(T - T_0) + \beta(\mathrm{RH} - \mathrm{RH}_0) \qquad (2)$$

where R_{ct_0} is the value of R_{ct} at a given temperature T_0 and relative humidity RH_0, and α and β are two constant coefficients.

The humidity dependence of R_{ct} is related to the interaction of the GO surface with water molecules,[15] which gives rise to protonation and hence to an increase in the density of charge carriers. In the case of thick films (thickness ≥ 1 μm), the constant phase element CPE2 can also play a relevant role, since its dependence on humidity reflects the onset and evolution of the diffusion regime for charge transport within the GO matrix. In ultrathin GO films the diffusion becomes negligible, so that the CPE2 element behaves like a bare resistor ($n_2 \sim 0$) and can be combined with the R_{ct} resistor in the analysis. Thus, in such a case, the equivalent circuit of Figure 1c becomes a parallel RC circuit where *R* is the only parameter sensitive to either RH or *T*, and the exponential dependence is readily observed by measuring the film's conductance. For example, in Figure 1d, we show the AC conductance *G* of a 15 nm thick spray-coated GO film as a function of RH at $T = 20$ °C, measured with an LCR meter at 10 kHz. It should be noticed that even ultrathin films exhibit an excellent dynamic range and full-scale output in humidity sensing.

The almost exponential behavior of the R_{ct} on humidity and temperature (within the range studied here) may be related to the superlinear dependence of GO permeability on the water vapor pressure,[14] resulting from the gradual opening of pores and insertion of water molecules within the GO film. Since the individual GO layers are interlinked *via* hydrogen bonding (H-bonds) between functional groups and water molecules, at high RH, the H-bonds between water molecules dominate causing an increase in the distance between the GO layers and a reduction of the intra- and interlayer H-bond interactions.[23] Furthermore, capillarity is likely to affect the behavior of water vapor within the nanometer-sized pores given by GO interlayer spacing.

The temperature dependence of GO impedance has been reported by Huang and coauthors[22] in the case of a GO paper (about 120 μm thick) and basically interpreted as a semiconductor-like behavior in the range 10−90 °C, due to presence of mobile ions. Thus, thermal activation of conductivity is reasonable to be observed also in GO thin films, and ascribable to the semi-insulating nature and to the morphology of the films, which is a network of overlapping nano- and microflakes. More specifically, charge transport is likely to take place *via* a hopping mechanism between adjacent polyaromatic molecules, like in the case of organic semiconductors. Also, the effect of temperature on the water vapor pressure is likely to play a relevant role.

A full comprehension of the combined role of *T* and RH would certainly deserve a deeper study (not the object of the present paper), in order to find a model able to accurately describe the behavior of GO electrical impedance and the effect of all the above-mentioned physical-chemical phenomena involved. However, the exponential approximation described in eq 2 is sufficient for sensing purposes, providing a facile way to decouple the humidity and temperature responses. As an example, the performance of a 15 nm thin GO sensor is reported in Figure 2 and directly compared to a high precision Vaisala HMT337 RH sensor. In this case, the sensor was calibrated by means of a humidity ramp and a temperature ramp in the environmental chamber; eq 2 was then used to transform the measured conductance values into RH values. A reference T sensor was used to compensate the *T* effect. Importantly, the calibration procedure required for such a sensor can be very easy and fast, due to the simple transfer function and the small number of unknown coefficients to be estimated (two coefficients, α and β), providing an advantage in terms of industrial scale-up. A better sensing performance in terms of accuracy may be achieved by using more complex functions (such as a sigmoidal, able to reproduce a saturation plateau at high RH values and a lower sensitivity at low RH values) to replace the exponential approximation; however, this would limit the simplicity of the calibration procedure. Also, a hysteresis effect is

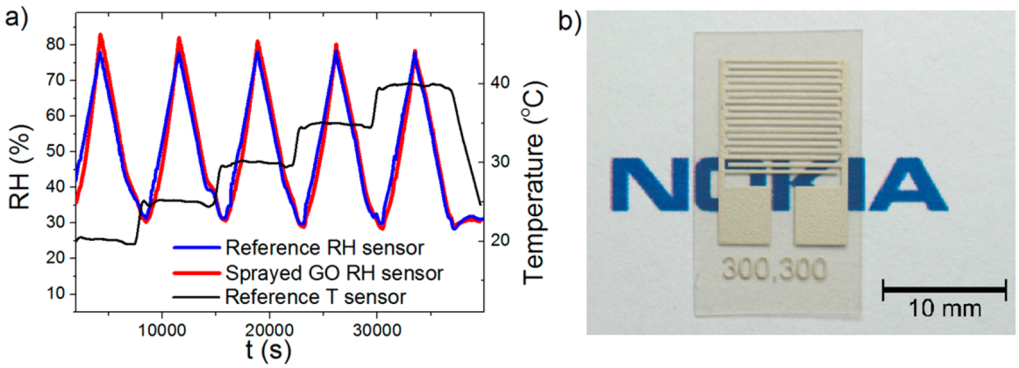

Figure 2. (a) Sensing performance of a 15 nm thick GO sensor (red line) compared to the response of a commercial high precision RH sensor (blue line). The AC resistance values of the GO sensor were converted into RH values using the function of eq 2 with the α, β and R_{ct0} parameters coming from calibration and the T values (black line) from a reference thermometer. (b) Photograph of a sprayed GO sensing element (only the printed Ag electrodes on top of the PEN substrate are visible, due to the transparency of the ultrathin GO film). (Logo published under permission.)

visible when RH is ramped from low to high values and back, limiting the sensing accuracy as visible in Figure 2.

Furthermore, the decoupling of the information about RH and T may be achieved by combining the response of two GO sensing elements with distinct α and β coefficients.[24] For example, we found that the coefficients could be tuned by pretreating the samples in oxygen plasma prior to GO deposition, probably due to a modification of the interface between the GO film and the electrodes that could affect the charge transport. Some other strategies to tune the α and β coefficients of the GO sensors in a controlled way, such as the functionalization of GO or the deposition of coatings on top of GO, are under study. Also, a study of the long-term stability of GO sensors is ongoing, motivated by the reported instability of GO in water.[15] Our preliminary results indicate that the conductance and sensitivity of GO sensors can be slightly affected by a prolonged high humidity cycle (*i.e.*, RH = 90% and T = 40 °C for 72 h).

Mechanical tests were also carried out to check the performance of the sensors in terms of flexibility. We verified that the sensor's response to RH was unaffected under flexure and after 1000 bending cycles to a bending radius of 10 mm (Supplementary Figure S10). Therefore, flexible RH sensors may be obtained on plastic substrates by low cost manufacturing processes. Also, fully transparent sensors were obtained by using either CVD graphene or ITO electrodes, with ultrathin GO films sprayed on top (see Supporting Information) with no evident departure from the performance shown above. However, screen printed Ag electrodes were used for the study of the sensors performance, due to the ease and speed of manufacture.

The thickness and morphology of the GO thin films, determined by the different preparation methods (see AFM and SEM analysis in the Supporting Information), influence the impedance spectrum and the sensors response, as demonstrated in the analysis so far. Due to the 2D nature of the GO material, an ultimate thinness is theoretically achievable, given by the thickness of a GO monolayer. In practice, we have verified that GO films averaging 15 nm in thickness can be easily and reproducibly obtained by spray coating, still keeping a decent sensitivity to RH (see Figure 1d). Such properties, together with the superpermeability to water, can allow the realization of ultrafast humidity sensors with unparalleled speed.

Ultrafast Sensing. The speed of GO-based humidity sensors was studied as a function of the GO film thickness. The performances of the three different types of GO films were compared, together with a fast commercial humidity sensor as a benchmark. To evaluate the response and recovery time of the sensors, we designed an experimental setup including a controlled humid air flow and a chopper to periodically interrupt the flow, with chopper frequency ranging from 1 to 80 Hz. Then, the sensors response S to the modulated humid flow was measured by means of a lock-in amplifier and an oscilloscope. The setup is shown in Figure 3a and fully described in the Methods section.

The response of each sensor was normalized with respect to the values measured at low humidity (S_L, humid flow interrupted) and high humidity (S_H, humid flow onto the sample): $S_N = (S - S_L)/(S_H - S_L)$. As shown in Figure 3b, already at the lowest frequency (1 Hz) the clear difference in the speed of the different sensors can be easily appreciated. In particular, only the sensors based on sprayed GO films were able to fully follow the humidity modulation, *i.e.*, display a normalized response ranging from 0 to 1. This same capability was kept by the thinnest GO films even at higher frequencies, as shown in Figure 3c for a 10 Hz modulation.

To better assess and compare the sensor performances, we captured a series of 10 s long traces at chopper frequencies ranging from 1 to 80 Hz for each sensor. We then carried out Fast Fourier Transforms (FFTs) of each trace, and evaluated the magnitude of the FFT at the chopper frequency to determine the

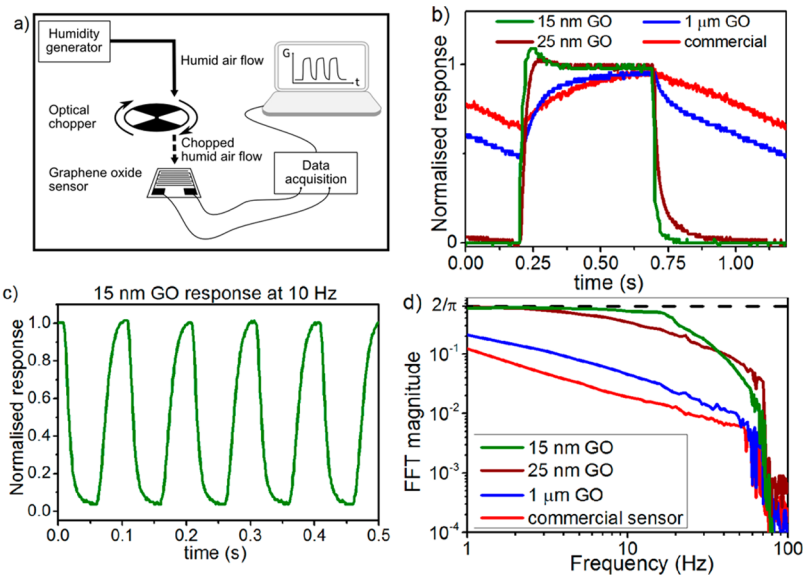

Figure 3. (a) Diagram of the experimental setup used to study the humidity sensors speed; (b) normalized response of the different sensors to a modulated humid air flow at 1 Hz; (c) normalized response of a 15 nm thick GO sensor to a modulated humid air flow at 10 Hz; (d) FFT magnitude of the response of different sensors to a modulated humid air flow as a function of the frequency.

fundamental frequency response of the sensor (shown as a Bode magnitude plot in Figure 3d).

Response and recovery times (defined as the time to go from 10% to 90% of the high humidity value and *vice versa*) less than 100 ms are clearly demonstrated from these measurements, with the thinnest films being able to respond up to 40−50 Hz. Also, the major role of thickness in tuning the response time of GO films is evident: the FFT analysis reported in Figure 3 shows that the response of the 25 nm thick film is clearly slower than that of the 15 nm one. Namely, typical response times were almost comparable (about 20−30 ms), whereas the recovery time was markedly longer for 25 nm thick films (90 ms compared to 30 ms for 15 nm thick films, shown in Figure S10 in Supporting Information).

The frequency roll-off for most sensors is approximately 20 dB/decade, which suggests a simple single-pole mechanism limits the sensor speed. The 15 nm sensor exhibits a steeper roll-off associated with a multi-pole mechanism, although the origin of this behavior is not understood at this time. Above frequencies of 60 Hz, the response becomes noisy and inconsistent; we believe that this is due to the humid air flow becoming turbulent at these chopper frequencies, rather than any fundamental limits within the sensors themselves.

Note that because the data was renormalized between zero (corresponding to the sensor response with no humid flow) and one (corresponding to the sensor response with constant humid flow), the maximum expected magnitude of the FFT for a perfect square wave response would be $2/\pi$ (shown as a dotted line in Figure 3d).

To our knowledge, these are the fastest humidity sensors ever reported. For example, ultrafast optical sensors based on optical fibers could show a very fast response (about 50 ms response time to go from the starting low humidity value to 90% of the new higher value) but a markedly slower recovery (>700 ms to recover from 90% to 20%).[25] Commercially available ultrafast optical sensor are reported to have a rise time (from 10% to 90%) limited to 100 ms.[26] Moreover, the simple electrical sensors reported here are remarkably advantageous with respect to any optical transducer in terms of ease of implementation in electronic systems.

Concerning electrical devices, the commercial sensors tested here as a benchmark represent the state-of-the-art of ultrafast capacitive sensors based on polymer thin films, with a minimum achievable time constant $T_{0.63}$ (*i.e.*, response time to get to 63% of the new value) of 100 ms declared in the specifications,[27] which would correspond to a rise time (from 10% to 90%) exceeding 200 ms assuming a single pole response. For example, a time constant $T_{0.63} < 1.5$ s is given in the specifications of another fast capacitive humidity sensor, measured when recovering from high to low humidity.[28] An ultrafast device based on polyelectrolyte fibers was claimed in ref 29, but only sensitive within a very limited range and at very low humidity (RH < 20%) and therefore useless for any practical application in ambient atmosphere.

Fast humidity sensors based on Surface Acoustic Wave were also reported, but both response and recovery time were of the order of 1 to 2 s.[30,31]

Thus, humidity sensors with optimized speed may be engineered at manufacturing, by tuning the GO films thickness. Moreover, ultrathin GO films, easily obtained by spray coating, display unparalleled speed both in response and recovery, being able to follow humidity modulation at frequencies of tens of Hz. This exceptional

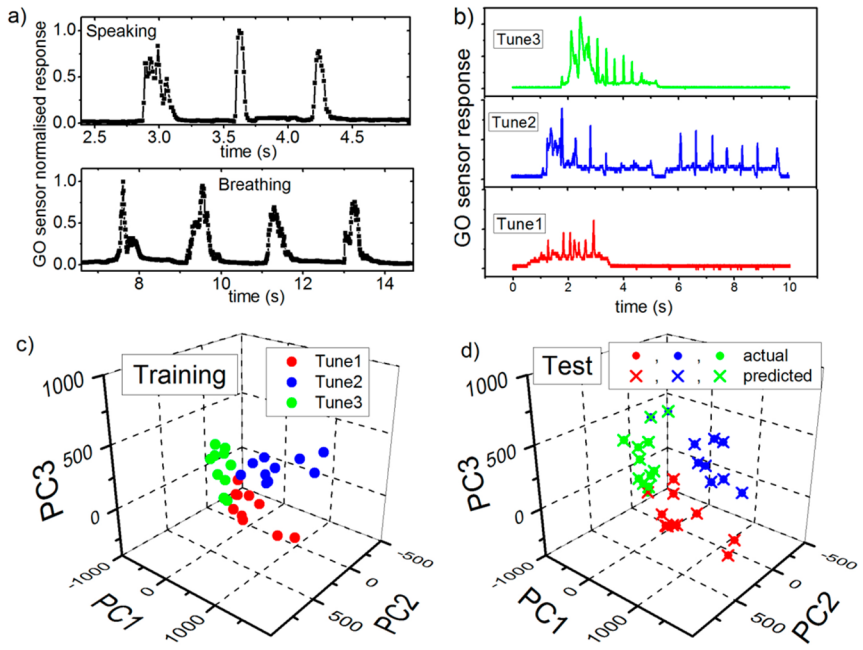

Figure 4. (a) GO sensor response to breathing and speaking, normalized to the maximum value in the traces; (b) responses of an ultrathin GO sensor to 3 different tunes whistled by three different users; (c) PCA analysis of the three tunes used to train the system; (d) Recognition of the tunes.

performance is intimately related to the peculiar nature of the 2D GO flakes, which can give rise to ultrathin porous films with superpermeability and high sensitivity toward water molecules. Unique water dynamics within randomly connected two-dimensional spaces were recently predicted by first-principles calculations.[32]

These ultrafast humidity sensors may enable novel applications, such as in breath monitoring or in the development of new user interfaces (UIs).[33] For example, the ability of a GO sensor in monitoring both breathing and speaking is shown in Figure 4. Particularly, it should be noticed that the ultrafast performance of the GO sensor allows the capture of fine features due to moisture modulation during the user's speech.

A potential application is showcased, where a GO ultrafast RH sensor is used to recognize different whistled tunes. As visible in Figure 4, the sensor was able to capture the fine patterns which are characteristics of each tune. Then, the traces were analyzed by FFT and Principal Components Analysis, and a clear clustering corresponding to the different tunes was obtained. Therefore, after training the system by 10 data points per tune (Figure 4c), each whistled tune could be classified and recognized with an accuracy of about 90% (Figure 4d), enabling user authentication by means of a low cost and low power sensor (see videos in the Supporting Information).

CONCLUSIONS

We have developed equivalent circuit models to describe the humidity and temperature dependent impedance spectra of GO thin films of varying thickness. We found that as the thickness of the GO films is decreased to 15 nm, the response to a modulated humid flow becomes ultrafast (~30 ms response and recovery times) while maintaining a full scale output of over an order of magnitude. This has led to the development of not only flexible and transparent sensors that are manufactured using low-cost, scalable processes but also what we believe to be the fastest humidity sensor yet reported. We can exploit the ultrafast response of thin GO films in new kinds of user interface based on moisture detection in a user's breath.

More generally, 2D materials may enable a new class of nanoporous thin films that exploit the unique advantages arising from the atomic thinness of the constituent sheets, the subnanometer pore sizes and facile manufacturing processes. On the basis of recent findings about chemical sensing properties of 2D materials,[34,35] such thin films may result suitable for applications in various fields such as consumers electronics, health and environmental monitoring.

METHODS

Graphene Oxide Films and Devices. Graphene oxide aqueous solutions (1 g/L, Graphene Square, Inc.) were deposited by either drop casting or spray coating. Drop casting was carried out using a micropipet (volume of deposited GO solution ~0.5 mL) with the substrate heated to 100 °C. Spray coating

was carried out using a handheld airbrush with compressed air as the propellant and with the substrate heated to 120 °C on a hot plate throughout.

Interdigitated Ag electrodes were screen printed using Dupont 5064H silver ink on Teonex PEN substrates (Teijin Dupont Films). Typical dimensions of the interdigitated electrodes were 300 μm electrode width, 300 μm electrode separation, 1 cm electrode length, and number of electrodes was 17 to give approximate channel width-to-length ratio as 570.

SEM characterization was carried out by means of a LEO 1530VP field-emission scanning electron microscope.

AFM measurements were performed in an Asylum Research MFP-3D Atomic Force Microscope in tapping mode.

Optical absorption measurements were performed using an Ocean Optics QE65000 spectrometer with a 50 μm spot size on GO films with various thicknesses deposited on transparent glass slides.

Plasma treatment of the samples prior to GO deposition (in order to tune the response to RH and T) was carried out in a Diener Femto plasma reactor in oxygen atmosphere (power = 50 W, flow rate = 20 sccm) for 2 min.

Impedance Measurements. The characterization of GO impedance as a function of RH and *T* was carried out in a Votsch VC4018 environmental chamber, equipped with additional Vaisala HMT337 sensors for high precision monitoring of the actual humidity and temperature within the chamber.

An Agilent 4294 impedance analyzer (frequency range 40 Hz to 110 MHz) was used to acquire GO impedance spectra, and a HP 4263A LCR meter for AC conductance measurements at 10 kHz.

The analysis and fitting of impedance spectra was carried out by means of EIS Spectrum Analyzer software.

Flexibility Tests. Bending tests were carried out on GO sprayed samples using a computer-controlled flex/stretch system, which could move in $+x$ and $-x$ direction uniaxially and therefore bend the samples to various radii of curvature. The samples were cycled up to 1000 times in steps of three bend radii: r = 30, 16, 10 mm.

Speed Evaluation. An OHG-4 Owlstone humidity generator was used to make a humid air flow with controlled and stable flow rate (450 sccm) and RH (75%).

The airflow was modulated by passing it through a Thorlabs MC2000 optical chopper wheel located between the humid air nozzle and the sensor.

The sensor response was measured using a Stanford Research SR830 lock-in amplifier and a Stanford Research SR570 low-noise current preamplifier: the lock-in provided a 1 V, 10 kHz excitation to one contact of the sensor, and the other contact was connected to the input of the preamplifier; the preamplifier output was then fed back to the lock-in amplifier input. We used high-bandwidth, 100 μA/V sensitivity settings on the preamplifier and a 1 ms lock-in time constant to ensure that there were no bandwidth limitations arising from the electronic measurement at the frequencies of interest. The magnitude of the lock-in reading was fed into a Lecroy LC334AM oscilloscope so that precise timings of the sensor response could be taken.

The commercial sensors used as a benchmark for ultrafast capacitive RH sensors were UPSI G-US.14R2 devices. Also Sensirion humidity sensors (model SHT71) were tested using their own acquisition electronics, but their response time (of the order of several seconds) was too slow to follow even the slowest (1 Hz) humid flow modulation.

Control experiments were carried out in order to rule out any response of the GO sensors to different stimuli other than humidity, such as pressure, light, mechanical deformation. When the humidity within the airflow was adjusted at about the value of the ambient humidity in the lab (about 40%), no response was observed, whereas a negative response (decrease of conductance) was observed when a dry airflow was blown on the sensors.

Principal Components Analysis. For the analysis of the whistled tunes, for each tune sample, a 10 s long trace was captured using the acquisition setup described in the Speed Evaluation section. Three individuals each whistled 20 sets of a distinct tune. We calculated the discrete Fourier transform of each trace, and took the absolute value to remove any phase-related information that may be due to the tunes not starting at exactly the same moment. Only the first hundred Fourier components were retained, as higher frequency components were predominantly caused by noise. Each set of tunes was then randomly split into 10 'training' tunes and 10 'test' tunes. Using MATLAB, we calculated the principal components of the training set of Fourier transforms by singular value decomposition. The test data was projected onto this principal component basis, and then we used linear discriminant analysis to classify the test tunes according to principal components found for the training group.

Conflict of Interest: The authors declare no competing financial interest.

Supporting Information Available: Details about GO films thickness evaluation, impedance spectra fitting, GO sensors performance; videos showing the whistling recognition performance of GO sensors. This material is available free of charge *via* the Internet at http://pubs.acs.org.

Acknowledgment. The authors would like to thank Mark Allen for help with screen-printing, Christopher Bower for carrying out the AFM characterization and Jan Mertens for performing the optical absorption measurements.

REFERENCES AND NOTES

1. Novoselov, K. S.; Jiang, D.; Schedin, F.; Booth, T. J.; Khotkevich, V. V.; Morozov, S. V.; Geim, A. K. Two-Dimensional Atomic Crystals. *Proc. Natl. Acad. Sci. U.S.A.* **2005**, *102*, 10451–10453.
2. Wang, Q. H.; Kalntar-Zadeh, K.; Kis, A.; Coleman, J. N.; Strano, M. S. Electronics and Optoelectronics of Two-Dimensional Transition Metal Dichalcogenides. *Nat. Nanotechnol.* **2012**, *7*, 699–712.
3. Lee, K. H.; Shin, H.-J.; Lee, J.; Lee, I.; Kim, G.-H.; Choi, J.-Y.; Kim, S.-W. Large-Scale Synthesis of High-Quality Hexagonal Boron Nitride Nanosheets for Large-Area Graphene Electronics. *Nano Lett.* **2012**, *12*, 714–718.
4. Bresnehan, M. S.; Hollander, M. J.; Wetherington, M.; LaBella, M.; Trumbull, K. A.; Cavalero, R.; Snyder, D. W.; Robinson, J. A. Integration of Hexagonal Boron Nitride with Quasi-Freestanding Epitaxial Graphene: Toward Wafer-Scale, High-Performance Devices. *ACS Nano* **2012**, *6*, 5234–5241.
5. Liu, Y.; Dong, X.; Chen, P. Biological and Chemical Sensors Based on Graphene Materials. *Chem. Soc. Rev.* **2012**, *41*, 2283–2307.
6. Mannoor, M. S.; Tao, H.; Clayton, J. D.; Sengupta, A.; Kaplan, D.; Naik, R. R.; Verma, N.; Omenetto, F. G.; McAlpine, M. C. Graphene-Based Wireless Bacteria Detection on Tooth Enamel. *Nat. Commun.* **2012**, *3*, 763.
7. Park, S. J.; Kwon, O. S.; Lee, S. H.; Song, H. S.; Park, T. H.; Jang, J. Ultrasensitive Flexible Graphene Based Field-Effect Transistor (FET)-Type Bioelectronic Nose. *Nano Lett.* **2012**, *12*, 5082–5090.
8. Kwak, Y. H.; Choi, D. S.; Kim, H.; Yoon, D. H.; Ahn, S. S.; Yang, J. W.; Seo, S. Flexible Glucose Sensor Using CVD-Grown Graphene-Based Field Effect Transistor. *Biosens. Bioelectron.* **2012**, *37*, 82–87.
9. Dreyer, D. R.; Park, S.; Bielawski, C. W.; Ruoff, R. S. The Chemistry of Graphene Oxide. *Chem. Soc. Rev.* **2010**, *39*, 228–240.
10. Brodie, B. Note sur un Nouveau Procede pour la Purification et la Pesagregation du Graphite. *Ann. Chim. Phys.* **1855**, *45*, 351–353.
11. Eda, G.; Chhowalla, M. Chemically Derived Graphene Oxide: Towards Large-Area Thin-Film Electronics and Optoelectronics. *Adv. Mater.* **2010**, *22*, 2392–2415.
12. Zhu, Y.; Murali, S.; Cai, W.; Li, X.; Suk, J. W.; Potts, J. R.; Ruoff, R. S. Graphene and Graphene Oxide: Synthesis, Properties, and Applications. *Adv. Mater.* **2010**, *22*, 3906–3924.
13. Dikin, D. A.; Stankovich, S.; Zimney, E. J.; Piner, R. D.; Dommett, G. H. B.; Evmenenko, G.; Nguyen, S. T.;

Ruoff, R. S. Preparation and Characterization of Graphene Oxide Paper. *Nature* **2007**, *448*, 457–460.
14. Nair, R. R.; Wu, H. A.; Jayaram, P. N.; Grigorieva, I. V.; Geim, A. K. Unimpeded Permeation of Water through Helium-Leak-Tight Graphene-Based Membranes. *Science* **2012**, *335*, 442–444.
15. Dimiev, A. M.; Alemany, L. B.; Tour, J. M. Graphene Oxide. Origin of Acidity, Its Instability in Water, and a New Dynamic Structural Model. *ACS Nano* **2013**, *7*, 576–588.
16. Yao, Y.; Chen, X.; Zhu, J.; Zeng, B.; Wu, Z.; Li, X. The Effect of Ambient Humidity on the Electrical Properties of Graphene Oxide Films. *Nanoscale Res. Lett.* **2012**, *7*, 363.
17. Zhao, C. L.; Qin, M.; Huang, Q. A. Humidity Sensing Properties of the Sensor Based on Graphene Oxide Films with Different Dispersion Concentrations. *2011 IEEE Sensors Proceedings*; IEEE: Red Hook, NY, 2011; pp 129−132.
18. Zhao, C. L.; Qin, M.; Li, W. H.; Huang, Q. A. Enhanced Performance of a CMOS Interdigital Capacitive Humidity Sensor by Graphene Oxide. *2011 16th International Solid-State Sensors, Actuators and Microsystems Conference (TRANSDUCERS 2011)*; IEEE: Red Hook, NY, 2011; pp 1954−1957.
19. Yao, Y.; Chen, X.; Guo, H.; Wu, Z. Graphene Oxide Thin Film Coated Quartz Crystal Microbalance for Humidity Detection. *Appl. Surf. Sci.* **2011**, *257*, 7778–7782.
20. Yao, Y.; Chen, X.; Guo, H.; Wu, Z.; Li, X. Humidity Sensing Behaviors of Graphene Oxide-Silicon Bi-layer Flexible Structure. *Sens. Actuators, B* **2012**, *161*, 1053–1058.
21. Guo, L.; Jiang, H.-B.; Shao, R.-Q.; Zhang, Y.-L.; Xie, S.-Y.; Wang, J.-N.; Li, X.-B.; Jiang, F.; Chen, Q.-D.; Zhang, T.; *et al.* Two-Beam Laser Interference Mediated Reduction, Patterning and Nanostructuring of Graphene Oxide for the Production of a Flexible Humidity Sensing Device. *Carbon* **2012**, *50*, 1667–1673.
22. Huang, X.; Zhi, C.; Jiang, P.; Golberg, D.; Bando, Y.; Tanaka, T. Temperature-Dependent Electrical Property Transition of Graphene Oxide Paper. *Nanotechnology* **2012**, *23*, 455705.
23. Medhekar, N. V.; Ramasubramaniam, A.; Ruoff, R. S.; Shenoy, V. B. Hydrogen Bond Networks in Graphene Oxide Composite Paper: Structure and Mechanical Properties. *ACS Nano* **2010**, *4*, 2300–2306.
24. Nokia Corporation. Patent application pending: U.S. 13/739,518, 2013.
25. Mathew, J.; Semenova, Y.; Farrell, G. A Fiber Bend Based Humidity Sensor with a Wide Linear Range and Fast Measurement Speed. *Sens Actuators, A* **2012**, *174*, 47–51.
26. NanoSonic NanoFP Optical Fiber-Based Humidity Sensor: http://www.nanosonic.com/80/14/nanofpopticalfiberbasedhumiditysensor.html.
27. UPSI sensors: http://www.upsi.fr/.
28. IST AG sensors: http://www.ist-ag.com/eh/ist-ag/en/home.nsf/contentview/∼humidity.
29. Berry, V.; Saraf, R. F. Modulation of Electron Tunneling in a Nanoparticle Array by Sound Waves: An Avenue to High Speed, High Sensitive Sensors. *Small* **2011**, *7*, 2485–2490.
30. Buvailo, A.; Xing, Y.; Hines, J.; Borguet, E. Thin Polymer Film Based Rapid Surface Acoustic Wave Humidity Sensors. *Sens. Actuators, B* **2011**, *156*, 444–449.
31. Lin, Q.; Li, Y.; Yang, M. Highly Sensitive and Ultrafast Response Surface Acoustic Wave Humidity Sensor Based on Electrospun Polyaniline/Poly(vinyl butyral) Nanofibers. *Anal. Chim. Acta* **2012**, *748*, 73–80.
32. Boukhvalov, D. W.; Katsnelson, M. I.; Son, Y.-W. Origin of the Anomalous Water Permeation Through Graphene Oxide Membrane. *Nano Lett.* **2013**, *13*, 3930–3935.
33. Nokia Corporation. Patent application pending: U.S. 13/747,729, 2013.
34. Prezioso, S.; Perrozzi, F.; Giancaterini, L.; Cantalini, C.; Treossi, E.; Palermo, V.; Nardone, M.; Santucci, S.; Ottaviano, L. Graphene Oxide as a Practical Solution to High Sensitivity Gas Sensing. *J. Phys. Chem. C* **2013**, *117*, 10683–10690.
35. Perkins, F. K.; Friedman, A. L.; Cobas, E.; Campbell, P. M.; Jernigan, G. G.; Tonker, B. T. Chemical Vapor Sensing with Monolayer MoS_2. *Nano Lett.* **2013**, *13*, 668–673.